Cooperative Effects in Molecular Conduction II: The Semiconductor−Metal Molecular Junction†

Arie Landau‡ and Abraham Nitzan*

School of Chemistry, Tel Aviv University, Tel Aviv 69978, Israel

Leeor Kronik

Department of Materials and Interfaces, Weizmann Institute of Science, Rehovoth 76100, Israel

Received: January 12, 2009; Revised Manuscript Received: March 1, 2009

Our recent calculation of the effect of intermolecular interactions on molecular conduction (*J. Comput. Theor. Nanosci.* **2008**, *5*, 535) is generalized to molecules adsorbed on a model semiconductor surface and in a metal−molecule−semiconductor junction. The metal and semiconductor electrodes are represented by cubic lattices within generic tight binding models, where the semiconductor two-band structure is described by using a simple site-alteration property. A physically motivated choice of parameters for the molecule(s) and the electrodes completes the model definition. The model encompasses direct intermolecular interactions as well as through-metal interactions and can be solved exactly to yield spectral properties (surface density of states) and transport characteristics (transmission coefficients and current−voltage behavior) for single-molecule junctions and molecular layers. The model is applied to analyzing the effect of intermolecular interactions on the predicted negative differential resistance in metal−molecule−semiconductor junctions (recently observed in scanning tunneling microscopy studies of adsorbates on Si(100)).

1. Introduction

Molecular electronic devices, potentially the next step in device miniaturization, are based on applying the electronic transport properties of molecular junctions to achieve functional goals. A molecular junction is made of at least two (metal (MET) or semiconductor (SC)) electrodes connected by a molecular spacer−a single molecule or a molecular layer. While most junctions investigated to date are based on metallic leads, the use of semiconductor electrodes offers potentially stronger bonding and a richer variety of behaviors associated with different band structures and doping levels. For these reasons, junctions comprising SC electrodes have come increasingly under study.[1−20] As subjects of computational work, such junctions are more challenging than their metallic counterparts mainly because essential properties of the pure semiconductor, such as its relevant band gap, are notoriously difficult to compute.[21] Furthermore, doped semiconductors are not easily amenable to direct ab initio calculations because their electronic behavior can be characterized only over the length and size scales typically not accessible to such calculations.

In this paper, we use a generalized tight binding model that comprises a molecule or a molecular layer adsorbed on and connecting between metal and SC surfaces in order to study the effect of intermolecular interactions on generic properties of molecular conduction in such junctions. This extends our previous study[22] of cooperative effects in molecular conduction in metal−molecule−metal junctions. The tight binding model for the MET electrode is described in ref 22. The SC is described, following Mujica and Ratner,[23] by a site-alteration nearest-neighbor tight binding model where a two-band solid is obtained by assigning different energies to neighboring sites. In one dimension, this yields a generalized Newns model[24] for the SC, for which the surface Green function (GF), self-energy (SE), and density of states (DOS) needed for transport calculations can be obtained analytically. Exact results for these functions for the three-dimensional analogue can be obtained numerically. They correspond to a two-band, one-gap SC model whose properties (band and gap widths) can be fit to actual systems by adjusting the site energies and the nearest-neighbor couplings. The molecule (m) or the molecular layer (ML) are modeled, as in ref 22, by a tight binding species (with parameters chosen as described in ref 22) adsorbed between these MET and SC model surfaces. The energetic and conduction properties of these models can be computed exactly, making it possible to compare these properties for a single molecule and for the molecular layer. In particular, the recent observation and analysis of negative differential resistance (NDR) in such junctions[7,8] is shown below to be very sensitive to intermolecular interactions in the transmitting molecular layer.

This article is organized as follows. In section 2, we analyze the one-dimensional tight-binding alternate-sites semiconductor model, with an adsorbed molecular species, and evaluate the needed surface GF, SE, and DOS. This sets the stage for the analogous computation of the corresponding three-dimensional model, for which a numerical approach is discussed in Sections 3 and 4. Section 5 discusses the chosen model parameters used in section 6 to compute the DOS, GFs, and SEs as well as transport properties of these junctions for both single-molecule and molecular layer junctions. Section 7 concludes.

2. Chemisorption on a One-Dimensional Model Semiconductor

Figure 1 shows a minimal model of a molecular site adsorbed on a one-dimensional semiconductor (SC) model described by

† Part of the "Robert Benny Gerber Festschrift".

* To whom correspondence should be addressed.

‡ Present address: Department of Chemistry, University of Southern California, Los Angeles, CA 90089-0482.

10.1021/jp900301f CCC: $40.75
Published on Web 04/06/2009

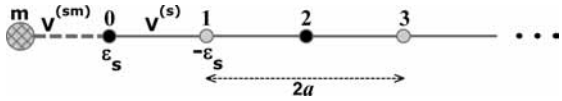

Figure 1. A schematic representation of a molecule m adsorbed on a one-dimensional semiconductor model characterized by a tight binding atomic chain of alternating positive and negative energy sites. The model is characterized by the site energies ε_s and ε_m and the nearest-neighbor coupling terms $V^{(s)}$ and $V^{(ms)}$. The lattice constant is $2a$.

a chain of repeated pairs of sites of energies ($\varepsilon_{s'}$, $-\varepsilon_s$) with a constant nearest-neighbor coupling $V^{(s)}$. The surface SC site is chosen arbitrarily to be of energy ε_s, and the molecular site is characterized by site energy ε_m and coupling to the SC surface site $V^{(sm)}$. The Hamiltonian is thus

$$\hat{H} = \varepsilon_m|m\rangle\langle m| + V^{(ms)}(|m\rangle\langle 0| + |0\rangle\langle m|) + \sum_{j=0}^{(N-2)/2}(\varepsilon_s|2j\rangle\langle 2j| - \varepsilon_s|2j+1\rangle\langle 2j+1|) + \sum_{j=0}^{N-2}(V^{(s)}|j\rangle\langle j+1| + \text{h.c.}) \quad (1)$$

where the SC sites are $j = 0, 1, 2,..., N-1$ (N is assumed even; below, we take $N \rightarrow \infty$), with even and odd position indices denoting sites of energies ε_s and $-\varepsilon_s$, respectively.

The spectral properties of this model can be evaluated analytically as an extension of the Newns procedure for the Newns−Anderson model.[24] This can be used to verify the numerical procedure described below for the analogous three-dimensional model.

Analytical Treatment. It is convenient to replace the local basis by one in which Bloch functions are used. Because there are two atoms per unit cell, the new basis involves a set of two independent Bloch functions that may be chosen in the forms

$$|\theta\rangle_e = \sqrt{\frac{4}{N}}\sum_{j=0}^{(N-2)/2}\sin\left[\left(j+\frac{1}{2}\right)2\theta\right]|2j\rangle \quad (2a)$$

$$|\theta\rangle_o = \sqrt{\frac{4}{N}}\sum_{j=0}^{(N-2)/2}\sin[(j+1)2\theta]|2j+1\rangle \quad (2b)$$

where $\theta \equiv ka$ and $k = n\pi/aN$ ($n = 1, 2,..., (N/2) - 1$); $|\theta\rangle_e$ and $|\theta\rangle_o$ contain contributions from the even and odd atomic sites, respectively. Equations 2a and 2b correspond to a chain of N atoms such that $\sin[((N-2)/2+1)2\theta] = 0$ for atom N. θ assumes values in the interval $0 \le \theta < \pi/2$, with the one-dimensional density of θ states given by

$$\rho_\theta = \frac{N}{\pi} \quad (3)$$

On the basis of these functions and assuming that $V^{(s)}$ is real, the Hamiltonian $\hat{H}$ satisfies

$$\langle\theta_e|H|\theta_e\rangle = \varepsilon_s \quad (4a)$$

$$\langle\theta_o|H|\theta_o\rangle = -\varepsilon_s \quad (4b)$$

$$\langle\theta_o|H|\theta_e\rangle = \langle\theta_e|H|\theta_o\rangle = 2V^{(s)}\cos(\theta) \quad (4c)$$

For any θ, the energy eigenvalues are obtained from the secular equation

$$\begin{vmatrix}\varepsilon_s - E_\theta & 2V^{(s)}\cos(\theta)\\ 2V^{(s)}\cos(\theta) & -\varepsilon_s - E_\theta\end{vmatrix} = 0 \quad (5)$$

which yields two bands

$$E_{\theta\pm} = \pm\sqrt{\varepsilon_s^2 + 4(V^{(s)})^2\cos^2(\theta)} \quad (6)$$

with the corresponding normalized eigenfunctions

$$|\theta_\pm\rangle = \frac{|\theta\rangle_e + \left(\frac{E_{\theta\pm} - \varepsilon_s}{2V^{(s)}\cos(\theta)}\right)|\theta\rangle_o}{\sqrt{1 + \frac{(E_{\theta\pm} - \varepsilon_{sc})^2}{4(V^{(s)})^2\cos^2(\theta)}}} \quad (7)$$

The spectral density that characterizes the interaction of the molecular level m with this 1-d model solid comprises additive contributions from these bands

$$\Gamma^{(m)}(E) = \Gamma_+^{(m)}(E) + \Gamma_-^{(m)}(E)$$
$$\Gamma_\pm^{(m)}(E) = 2\pi\sum_m |V_\pm^{(m\theta)}|^2\delta(E - E_{\theta\pm}) \quad (8)$$

The molecule (site m in Figure 1) interacts only with the "surface" atom (site 0). Consequently, $V_\pm^{(m\theta)} = V^{(ms)}\langle 0|\theta_\pm\rangle$. Using eqs 2a and 7 and then converting sum to integral using eq 3 yields

$$\Gamma_\pm^{(m)}(E) = \left(\frac{8\pi|V^{(ms)}|^2}{N}\right)\sum_\theta \frac{4(V^{(s)})^2\cos^2(\theta)\sin^2(\theta)}{(E_{\theta\pm} - \varepsilon_s)^2 + 4(V^{(s)})^2\cos^2(\theta)}\delta(E - E_{\theta\pm}) = 8|V^{(ms)}|^2\int_0^{\pi/2} d\theta \frac{4(V^{(s)})^2\cos^2(\theta)\sin^2(\theta)}{(E_{\theta\pm} - \varepsilon_s)^2 + 4(V^{(s)})^2\cos^2(\theta)}\delta(E - E_{\theta\pm}) \quad (9)$$

Changing the integration variable to E_θ using eq 6 (see Appendix A) and defining

$$b(E) = \frac{E^2 - \varepsilon_s^2}{4(V^{(s)})^2} \quad (10)$$

where eq 6 implies that $|b(E)| \le 1$ for E in the bands, finally leads to

$$\Gamma^{(m)}(E) = \begin{cases} \dfrac{4|V^{(ms)}|^2\sqrt{b(E) - b^2(E)}}{E - \varepsilon_s} & \text{for } \varepsilon_s \le E < \sqrt{\varepsilon_s^2 + 4(V^{(s)})^2} \\ \dfrac{4|V^{(ms)}|^2\sqrt{b(E) - b^2(E)}}{\varepsilon_s - E} & \text{for } -\sqrt{\varepsilon_s^2 + 4(V^{(s)})^2} \le E < -\varepsilon_s \\ 0 & \text{otherwise} \end{cases} \tag{11}$$

Two comments are in order. First, turning off the site energy alteration, that is, setting $\varepsilon_s = 0$ in eq 11, recovers the Newns semielliptic spectral density function[24] for the corresponding 1-d metal model. Second, the exact result eq 11 differs qualitatively from that obtained for this model in ref 23 and, in contrast to the latter, shows an asymmetric dependence on $E(\Gamma^{(m)}(E) \neq \Gamma^{(m)}(-E))$ that reflects the symmetry breaking associated with the molecular adsorption on either the positive or the negative energy SC site. Indeed, the symmetry property is $\Gamma^{(m)}(E,\varepsilon_s) = \Gamma^{(m)}(-E,-\varepsilon_s)$, which expresses the fact that the spectral density of a molecule adsorbed on a positive energy site is the mirror image of that of a molecule adsorbed on a negative energy site.

Numerical Evaluation. In what follows, we evaluate the surface Green function and self-energy using the numerical procedure described in ref 22, which is based on the renormalization group method[25−28] used earlier for evaluating tunneling electron fluxes through molecules and molecular layers.[29] We start by writing the Hamiltonian (eq 1) in the form

$$\hat{H} = \begin{pmatrix} H_m & \hat{H}_{ms} & 0 & \ldots \\ \hat{H}_{sm} & \hat{H}_{00} & \hat{H}_{01} & \ldots \\ 0 & \hat{H}_{10} & \hat{H}_{00} & \ldots \\ \ldots & \ldots & \ldots & \ldots \end{pmatrix} \tag{12}$$

where the molecular part is

$$H_m = \varepsilon_m \tag{13}$$

The 1-d semiconductor is represented by a repeated structure of two-dimensional matrices describing the unit cells and the coupling between them

$$\hat{H}_{00} = \begin{pmatrix} \varepsilon_s & V^{(s)} \\ V^{(s)*} & -\varepsilon_s \end{pmatrix} \tag{14}$$

$$\hat{H}_{01} = \begin{pmatrix} 0 & 0 \\ V^{(s)} & 0 \end{pmatrix} \qquad \hat{H}_{10} = \begin{pmatrix} 0 & V^{(s)*} \\ 0 & 0 \end{pmatrix} \tag{15}$$

and the molecule−SC coupling is given by

$$\hat{H}_{ms} = (V^{(ms)} \quad 0) \qquad \hat{H}_{sm} = (\hat{H}_{ms})^{\dagger} \tag{16}$$

For the bare one-dimensional SC, the surface Green function, $\hat{G}^{(ss)}$, and self-energy, $\hat{\Sigma}^{(ss)}$, satisfy

$$\begin{aligned} \hat{G}^{(ss)}(E) &= (E\hat{I} - \hat{H}_{00} - \hat{\Sigma}^{(ss)}(E))^{-1} \\ \hat{\Sigma}^{(ss)}(E) &= \hat{H}_{01}\hat{G}^{(ss)}(E)\hat{H}_{10} \end{aligned} \tag{17}$$

which yields a closed equation for the SE matrix

$$\Sigma^{(ss)}(E) = H_{01}(E\hat{I} - \hat{H}_{00} - \hat{\Sigma}^{(ss)}(E))^{-1}\hat{H}_{10} \tag{18}$$

where $\hat{I}$ is a 2 × 2 unity matrix. This equation is solved by the iterative renormalization-group technique.[25−27] Once a converged solution is reached, the molecular GF and SE are obtained from

$$\Sigma^{(m)}(E) = H_{ms}\hat{G}^{(ss)}(E)H_{sm} \tag{19a}$$

$$G^{(m)}(E) = (E - \varepsilon_m - \Sigma^{(m)}(E))^{-1} \tag{19b}$$

and the molecular spectral density is given by

$$\Gamma^{(m)}(E) = -2\,\mathrm{Im}(\Sigma^{(m)}(E)) \tag{20}$$

Note that the SC bulk GF is obtained in the same way in the form

$$G^{(b)}(E) = (E - H_{00} - \Sigma^{(ss)}(E) - (\Sigma^{(ss)}(E))^{\dagger})^{-1} \tag{21}$$

The density of states (DOS) functions associated with the molecule, the SC surface, and the SC bulk are given, respectively, by

$$\rho^{(m)}(E) = -\frac{1}{\pi}\,\mathrm{Im}[G^{(m)}(E)] \tag{22}$$

$$\rho^{(ss)}(E) = -\frac{1}{\pi}\,\mathrm{Im}[G^{(ss)}(E)] \tag{23}$$

$$\rho^{(b)}(E) = -\frac{1}{\pi}\,\mathrm{Im}[G^{(b)}(E)] \tag{24}$$

Results obtained from this numerical procedure are in complete agreement with the analytical results obtained above. A generalization of this procedure is however our main tool in the three-dimensional case.

3. Chemisorption on a Three-Dimensional Cubic Model Semiconductor

Hamiltonian. Consider a molecular monolayer chemisorbed on the surface of a 3-d site-alteration SC electrode, as represented schematically in Figure 2. The adsorbed layer and the SC are represented by single-site species placed on a simple cubic lattice, which is semi-infinite in the z direction and with periodic boundary in the x and y directions. A lattice site is described by (n_x,n_y,n_z), with $n_x = -N_x, -N_x + 1,..., N_x - 1$; $n_y = -N_y, -N_y + 1,..., N_y - 1$; and $n_z = 0, 1,..., \infty$. The SC surface is indexed as $n_z = 1$, and the molecular layer occupies positions on the $n_z = 0$ plane. This structure corresponds to the simplest commensurate molecular layer; more complex structures can be accounted for as described in ref 22. A simple tight binding model is considered, where each SC atom and each adsorbate molecule are represented by a single orbital, denoted $|n_x,n_y,n_z\rangle$, coupled to its nearest-neighbor orbitals. The interaction between nearest-neighbor SC atoms is denoted by $V^{(s)}$, and between adsorbate and SC sites, it is denoted by $V^{(ms-)}$ and $V^{(ms+)}$

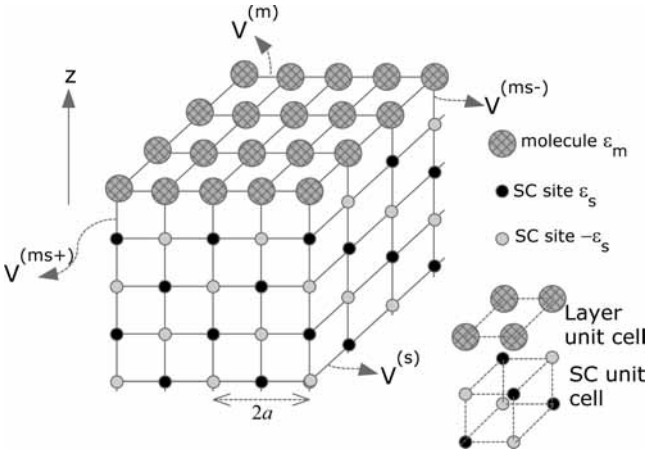

Figure 2. A three-dimensional schematic representation of a molecular layer adsorbed on a site-alternating SC surface. The SC sites of energies ε_s and $-\varepsilon_s$ are shown as small dark and light circles, and the molecular sites are shown as larger circles. Also shown are the unit cells (of dimension $2a$) that characterize the molecular and SC lattices. The tight coupling parameters are the intermolecular coupling $V^{(m)}$, the SC coupling $V^{(s)}$, and the molecular couplings $V^{(ms+)}$ and $V^{(ms-)}$ to the positive and negative energy SC sites, repectively.

for the negative and positive energy SC sites, respectively. The Hamiltonian is then

$$\hat{H} = \hat{H}^{SC} + \hat{H}^{ML} + \hat{H}^{ML-SC} \tag{25}$$

with the SC Hamiltonian, $\hat{H}^{SC}$, the molecular layer Hamiltonian, $\hat{H}^{ML}$, and their mutual interaction, $\hat{H}^{ML-SC}$, given by

$$\begin{aligned} H^{SC} = {} & \varepsilon_s \sum_{n_x=(-N_x/2)}^{(N_x/2)-1} \sum_{n_y=(-N_y/2)}^{(N_y/2)-1} \sum_{n_z=0}^{\infty} [|2n_x2n_y2n_z\rangle\langle 2n_x2n_y2n_z| + \\ & |(2n_x+1)(2n_y+1)2n_z\rangle\langle(2n_x+1)(2n_y+1)2n_z| + \\ & |(2n_x+1)2n_y(2n_z+1)\rangle\langle(2n_x+1)2n_y(2n_z+1)| + \\ & |2n_x(2n_y+1)(2n_z+1)\rangle\langle 2n_x(2n_y+1)(2n_z+1)|] - \\ & \varepsilon_s \sum_{n_x=(-N_x/2)}^{(N_x/2)-1} \sum_{n_y=(-N_y/2)}^{(N_y/2)-1} \sum_{n_z=0}^{\infty} [|(2n_x+1)2n_y2n_z\rangle\langle(2n_x+ \\ & 1)2n_y2n_z| + |2n_x(2n_y+1)2n_z\rangle\langle 2n_x(2n_y+1)2n_z| + \\ & |2n_x2n_y(2n_z+1)\rangle\langle 2n_x2n_y(2n_z+1)| + |(2n_x+1)(2n_y+ \\ & 1)(2n_z+1)\rangle\langle(2n_x+1)(2n_y+1)(2n_z+1)|] + \\ & V^{(s)} \sum_{n_x=-N_x}^{N_x-2} \sum_{n_y=-N_y}^{N_y-2} \sum_{n_z=0}^{\infty} [|n_xn_yn_z\rangle\langle n_xn_y(n_z+1)| + \text{h.c.} + \\ & |n_xn_yn_z\rangle\langle n_x(n_y+1)n_z| + \text{h.c.} + |n_xn_yn_z\rangle\langle(n_x+1)n_yn_z| + \\ & \text{h.c.}] \end{aligned} \tag{26}$$

$$\begin{aligned} H^{ML} = {} & \varepsilon_m \sum_{n_x=-N_x}^{N_x-1} \sum_{n_y=-N_y}^{N_y-1} |n_xn_y(n_z=0)\rangle\langle n_xn_y(n_z=0)| + \\ & V^{(m)} \sum_{n_x=-N_x}^{N_x-2} \sum_{n_y=-N_y}^{N_y-2} [|n_xn_y(n_z=0)\rangle\langle n_x(n_y+1)(n_z=0)| + \\ & \text{h.c.} + |n_xn_y(n_z=0)\rangle\langle(n_x+1)n_y(n_z=0)| + \text{h.c.}] \end{aligned} \tag{27}$$

and

$$\begin{aligned} H^{ML-SC} = {} & V^{(ms+)} \sum_{n_x=(-N_x/2)}^{(N_x/2)-1} \sum_{n_y=(-N_y/2)}^{(N_y/2)-1} [|2n_x2n_y(n_z= \\ & 0)\rangle\langle 2n_x2n_y(n_z=1)| + |(2n_x+1)(2n_y+1)(n_z= \\ & 0)\rangle\langle(2n_x+1)(2n_y+1)(n_z=1)| + \text{h.c.}] + \\ & V^{(ms-)} \sum_{n_x=(-N_x/2)}^{(N_x/2)-1} \sum_{n_y=(-N_y/2)}^{(N_y/2)-1} [|(2n_x+1)2n_y(n_z=0)_z\rangle\langle(2n_x+ \\ & 1)2n_y(n_z=1)| + |2n_x(2n_y+1)(n_z=0)\rangle\langle 2n_x(2n_y+ \\ & 1)(n_z=1)| + \text{h.c.}] \end{aligned} \tag{28}$$

with periodic boundary conditions in the $x-y$ plane.

In eqs 26−28, $|n_xn_yn_z\rangle$ denotes the orbital associated with the species on the corresponding site. It is convenient to use instead an enumeration of these orbitals in terms of the unit cell and its internal structure, $|n_xn_yn_z\rangle \rightarrow |\alpha;m_xm_ym_z\rangle$, where m_j, $j = x, y, z$ are unit cell indices and α denotes atoms in the unit cell (four in the molecular layer and eight in the underlying SC; see Figure 2). The corresponding Bloch functions in the xy plane are defined by

$$\begin{aligned} & |\alpha;\theta_x\theta_ym_z\rangle = \\ & \frac{1}{\sqrt{M_xM_y}} \sum_{m_x=(-M_x/2)}^{(M_x/2)-1} \sum_{m_y=(-M_y/2)}^{(M_y/2)-1} e^{i(2\theta_xm_x+2\theta_ym_y)} |\alpha;m_xm_ym_z\rangle \end{aligned} \tag{29}$$

Again, periodic boundary conditions are implied, with periods $M_u = N_u/2$ ($u = x, y$). Consequently, $\theta_u \equiv k_ua$ ($u = x, y$), where a is the interatomic distance ($2a$ is the unit cell size; see Figure 2) and $k_u = (\pi l/aM_u)$ ($l = 1, 2,..., M_u \rightarrow 0 < \theta_u \leq \pi$). In the basis of these Bloch functions, the Hamiltonian is block diagonal

$$\mathbf{H} = \begin{pmatrix} \mathbf{H}_{\boldsymbol{\theta}_{xy}} & 0 & 0 & ... \\ 0 & \mathbf{H}_{\boldsymbol{\theta}'_{xy}} & 0 & ... \\ 0 & 0 & \mathbf{H}_{\boldsymbol{\theta}''_{xy}} & ... \\ ... & ... & ... & ... \end{pmatrix} \tag{30}$$

where we have denoted $\boldsymbol{\theta}_{xy} = (\theta_x,\theta_y)$ and where each block on the diagonal represents a one-dimensional problem in the z direction and has the form

$$\mathbf{H}_{\boldsymbol{\theta}_{xy}} = \begin{pmatrix} \mathbf{H}^{ML}(\boldsymbol{\theta}_{xy}) & \mathbf{H}^{MS} & 0 & 0 & ... \\ \mathbf{H}^{MS\dagger} & \mathbf{H}^{SC}_{00}(\boldsymbol{\theta}_{xy}) & \mathbf{H}^{SC}_{01} & 0 & ... \\ 0 & \mathbf{H}^{SC}_{10} & \mathbf{H}^{SC}_{00}(\boldsymbol{\theta}_{xy}) & \mathbf{H}^{SC}_{01} & ... \\ 0 & 0 & \mathbf{H}^{SC}_{10} & \mathbf{H}^{SC}_{00}(\boldsymbol{\theta}_{xy}) & ... \\ ... & ... & ... & ... & ... \end{pmatrix} \tag{31}$$

Each block in the Hamiltonian matrix (eq 31) corresponds to the internal structure of unit cells and their mutual coupling as reflected in Bloch space. In particular, $\mathbf{H}^{SC}_{00}(\boldsymbol{\theta}_{xy})$ and $\mathbf{H}^{SC}_{01} = \mathbf{H}^{SC\dagger}_{10}$ are, respectively, diagonal and nondiagonal contributions (of dimensions 8×8) to the SC Hamiltonian, while $\mathbf{H}^{ML}(\boldsymbol{\theta}_{xy})$ and $\mathbf{H}^{MS}$ are, respectively, blocks of the Hamiltonian matrix of dimensions 4×4 and 4×8 corresponding to a unit cell of the adsorbed monolayer and its interaction with the SC cell below. Explicit forms of these Hamiltonians are given in Appendix B.

Self-Energy and Density of States for an Adsorbed Molecular Layer. Next, we use the scheme of ref 22 to compute the self-energy and spectral density associated with an adsorbate site. The equations analogous to eqs 18−20 now are the *k*-space functions

$$\Sigma^{SS}_{\boldsymbol{\theta}_{xy}}(E) = \mathbf{H}^{SC}_{01}(E\hat{I} - \mathbf{H}^{SC}_{00}(\boldsymbol{\theta}_{xy}) - \Sigma^{SS}_{\boldsymbol{\theta}_{xy}}(E))^{-1}\mathbf{H}^{SC}_{10} \quad (32)$$

which determine the SC surface SE

$$\Sigma^{ML}_{\boldsymbol{\theta}_{xy}}(E) = \mathbf{H}^{MS}(E\hat{I} - \mathbf{H}^{ML}(\boldsymbol{\theta}_{xy}) - \Sigma^{SS}_{\boldsymbol{\theta}_{xy}}(E))^{-1}\mathbf{H}^{\dagger MS} \quad (33)$$

which yields the molecular layer SE, and

$$\Gamma^{ML}_{\boldsymbol{\theta}_{xy}}(E) = \mathrm{i}(\Sigma^{ML}_{\boldsymbol{\theta}_{xy}}(E) - (\Sigma^{ML}_{\boldsymbol{\theta}_{xy}}(E))^{\dagger}) \quad (34)$$

is the molecular layer spectral density. $\hat{I}$ is a 4 × 4 or 8 × 8 unity matrix for the ML or SC, respectively. The semiconductor surface GF and the molecular layer GF (analogues of eqs 17 and 19b) are given by

$$G^{SS}_{\boldsymbol{\theta}_{xy}}(E) = (E\hat{I} - \mathbf{H}^{SC}_{00}(\boldsymbol{\theta}_{xy}) - \Sigma^{SS}_{\boldsymbol{\theta}_{xy}}(E))^{-1} \quad (35)$$

$$G^{ML}_{\boldsymbol{\theta}_{xy}}(E) = (E\hat{I} - \mathbf{H}^{ML}(\boldsymbol{\theta}_{xy}) - \Sigma^{ML}_{\boldsymbol{\theta}_{xy}}(E))^{-1} \quad (36)$$

For completeness, we note that the SC bulk Green function, that is, the analogue of eq 21, is given by $G^{B}_{\boldsymbol{\theta}_{xy}}(E) = (E\hat{I} - \mathbf{H}^{SC}_{00}(\boldsymbol{\theta}_{xy}) - \Sigma^{SS}_{\boldsymbol{\theta}_{xy}}(E) - (\Sigma^{SS}_{\boldsymbol{\theta}_{xy}}(E))^{\dagger})^{-1}$. The corresponding position space functions are obtained by a two-dimensional Fourier transform

$$X_{\mathbf{n}_{xy},\mathbf{n}'_{xy}}(E) = \frac{1}{4\pi^2}\int_0^{\pi}\int_0^{\pi} \mathrm{d}\theta_x \mathrm{d}\theta_y\, X_{\boldsymbol{\theta}_{xy}}(E)\mathrm{e}^{\mathrm{i}\boldsymbol{\theta}_{xy}\Delta\mathbf{n}_{xy}} \quad (37)$$

where $X = \Sigma, \Gamma, G$, $\mathbf{n}_{xy} \equiv (n_x,n_y)$, and $\Delta\mathbf{n}_{xy} = (n_x - n_x',n_y - n_y')$ and where the dependence on n_z has been omitted here and below for simplicity of presentation. In particular, the local GFs can be used to evaluate the density of states per site of the SC bulk, the SC surface, and an adsorbed molecule

$$\rho^{B}(E) = -\frac{1}{\pi}\,\mathrm{Im}[G^{B}_{\mathbf{n}_{xy},\mathbf{n}_{xy}}(E)] \quad (38a)$$

$$\rho^{SS}(E) = -\frac{1}{\pi}\,\mathrm{Im}[G^{SS}_{\mathbf{n}_{xy},\mathbf{n}_{xy}}(E)] \quad (38b)$$

$$\rho^{ML}(E) = -\frac{1}{\pi}\,\mathrm{Im}[G^{ML}_{\mathbf{n}_{xy},\mathbf{n}_{xy}}(E)] \quad (38c)$$

A Single Adsorbed Molecule. If instead of a molecular layer we have a single molecular adsorbate, the corresponding GF, self-energy, and spectral density are given by[22]

$$G^{m}_{\mathbf{n}_{xy},\mathbf{n}_{xy}}(E) = (E - \varepsilon_m - \Sigma^{m}_{\mathbf{n}_{xy},\mathbf{n}_{xy}}(E))^{-1} \quad (39a)$$

$$\Sigma^{m}_{\mathbf{n}_{xy},\mathbf{n}_{xy}}(E) = V^{(ms)\dagger}G^{SS}_{\mathbf{n}_{xy},\mathbf{n}_{xy}}V^{(ms)} \quad (39b)$$

$$\Gamma^{m}_{\mathbf{n}_{xy},\mathbf{n}_{xy}}(E) = \mathrm{i}(\Sigma^{m}_{\mathbf{n}_{xy},\mathbf{n}_{xy}}(E) - (\Sigma^{m}_{\mathbf{n}_{xy},\mathbf{n}_{xy}}(E))^{\dagger}) \quad (39c)$$

and, again, the density of states associated with the adsorbate

$$\rho^{(m)}(E) = -\frac{1}{\pi}\,\mathrm{Im}[G^{m}_{\mathbf{n}_{xy},\mathbf{n}_{xy}}(E)] \quad (40)$$

4. Conduction in a SC−Molecule−Metal Junction

Section 3 provides the surface GF and spectral properties associated with a single molecule or a molecular layer adsorbed on a model SC surface, based on a generalization of similar expressions derived in ref 22 for a model metal surface. These expressions can now be used to evaluate transmission and current−voltage characteristics of a metal−molecule−semiconductor junction based on these models. The needed expressions are generalizations of those derived in ref 22 and are summarized below.

Consider an adsorbate monolayer connecting between the metal (see ref 22) and semiconductor systems. The monolayer GF in Bloch space has a form similar to eq 36, except that the SE term combines additively contributions from both electrodes

$$G^{ML}_{\boldsymbol{\theta}_{xy}}(E) = (E\hat{I} - \mathbf{H}^{ML}(\boldsymbol{\theta}_{xy}) - {}^{SC}\Sigma^{ML}_{\boldsymbol{\theta}_{xy}}(E) - {}^{mtl}\Sigma^{ML}_{\boldsymbol{\theta}_{xy}}(E))^{-1} \quad (41)$$

where ${}^{SC}\Sigma^{ML}_{\boldsymbol{\theta}_{xy}}(E)$, the SC contribution, is given by eq 33 and ${}^{mtl}\Sigma^{ML}_{\boldsymbol{\theta}_{xy}}(E)$ is the corresponding contribution from the metallic electrode (eq 14 in ref 22). The transmission per molecule is given by (cf. eq 28 of ref 22)

$$\mathscr{T}^{ML}(E) = \frac{1}{4\pi^2}\,\mathrm{Tr}\Big[\int_0^{\pi}\int_0^{\pi}\mathrm{d}\theta_x\mathrm{d}\theta y\, {}^{SC}\Gamma^{ML}_{\boldsymbol{\theta}_{xy}}(E)G^{ML}_{\boldsymbol{\theta}_{xy}}(E)^{mtl}\Gamma^{ML}_{\boldsymbol{\theta}_{xy}}(E)(G^{ML}_{\boldsymbol{\theta}_{xy}}(E))^{\dagger}\Big] \quad (42)$$

where Tr denotes the trace operation and the spectral densities ${}^{SC}\Gamma^{ML}_{\boldsymbol{\theta}_{xy}}(E)$ and ${}^{mtl}\Gamma^{ML}_{\boldsymbol{\theta}_{xy}}(E)$ are given, respectively, by eq 34 above and eq 14 in ref 22.

Next, consider a single adsorbate species, taken to occupy the single site (n_x, n_y, $n_z = 0$) on the adsorbate plane $z = 0$. The adsorbate Green function, eq 39a, now takes the form[22]

$$G^{m}_{\mathbf{n}_{xy},\mathbf{n}_{xy}}(E) = (E - \varepsilon_m - {}^{SC}\Sigma^{m}_{\mathbf{n}_{xy},\mathbf{n}_{xy}}(E) - {}^{mtl}\Sigma^{m}_{\mathbf{n}_{xy},\mathbf{n}_{xy}}(E))^{-1} \quad (43)$$

where the SC and metal contributions to the self-energy are given by eq 39b and eq 23 in ref 22, respectively. The corresponding single-molecule transmission function is given by eq 27 in ref 22

$$\mathscr{T}^{m}(E) = {}^{SC}\Gamma^{m}_{\mathbf{n}_{xy},\mathbf{n}_{xy}}(E)G^{m}_{\mathbf{n}_{xy},\mathbf{n}_{xy}}(E)^{mtl}\Gamma^{m}_{\mathbf{n}_{xy},\mathbf{n}_{xy}}(E)(G^{m}_{\mathbf{n}_{xy},\mathbf{n}_{xy}}(E))^{\dagger} \quad (44)$$

In eq 44, the spectral densities ${}^{SC}\Gamma^{m}_{\mathbf{n}_{xy},\mathbf{n}_{xy}}(E)$ and ${}^{mtl}\Gamma^{m}_{\mathbf{n}_{xy},\mathbf{n}_{xy}}(E)$ are given by eq 39c and eq 23 in ref 22, respectively.

Once the transmission functions have been evaluated, the current in a biased junction can be obtained from the Landauer formula, using $\mathcal{T} = \mathcal{T}^{m}$ or $\mathcal{T}^{ML}$

$$I(\Phi) = \int dE(f_{mtl}(E) - f_{SC}(E))\mathcal{T}(E,\Phi) \qquad (45)$$

where $f(E)$ are the Fermi functions of the leads and the dependence on the electrostatic potential Φ is manifested by the potentials on the two electrodes as well by the way the potential bias falls across the junction. In the calculations reported below, we set the potential on the SC to 0 and the metal potential to Φ. The metal site energies in the absence of bias as well as the SC mid-band gap are taken as 0 in the unbiased junction. In the presence of bias Φ, the metal site energies are shifted to $-e\Phi$, and the molecular site energy is then taken to be

$$\varepsilon_m(\Phi) = \varepsilon_m(0) - Se\Phi \qquad (46)$$

The parameter S, $0 \le S \le 1$, is the molecular shift parameter that reflects the way by which the bias potential is distributed along the molecular bridge. $S \ll 1$ corresponds to a molecule bound strongly to the SC, whereas $S \sim 1$ implies stronger coupling to the metal electrode.

5. Model Parameters

The metal−molecule−SC model presented above depends on a number of energetic parameters. In the calculations shown and discussed in section 6, we use a set of such parameters that were estimated from experimental and computational data. In the following we present these estimates. Note that parameters associated with the molecule and metal subsystems, described in ref 22, were adopted again here.

(a) The SC site energy, $\pm\varepsilon_s$, is chosen to fit a desired band gap ($2\varepsilon_s$). We use $\varepsilon_s = \pm 0.215$ eV, which gives a 0.43 eV band gap, comparable to that of InAs.

(b) The SC tight binding interaction parameter $V^{(s)}$ determines the bandwidth. In particular, in the site-alteration model, the valence band encompasses the range $-2V^{(s)}d$ to $-\varepsilon_s$, and the conduction band lies between ε_s and $2V^{(s)}d$, where d is the dimensionality. Experimentally observed valence bandwidths are typically $W_V \sim 4$ eV,[30,31] and conduction bandwidths are of similar order, $W_C \sim 2-4$ eV.[31] Consequently, $V^{(s)}$ should be on the order of a few tenths of eV. Below, we use $V^{(s)} = 0.03$ au ~ 0.82 eV.

(c) The molecule−SC tight binding interaction parameter, $V^{(ms)}$, can be estimated from experimental measured lifetimes of excess electron transfer from the molecule to a SC surface, $\tau \sim 10-100$ fs.[32] This lifetime provides an estimate of $\Gamma^{(m)} = 2\pi|V^{(ms)}|^2\rho^{(s)}$, where $\rho^{(s)}$ is the SC DOS. The latter was estimated, using the SC DOS from Figure 5, to be $2\pi\rho^{(s)} \sim 1$ [eV]$^{-1}$. This implies coupling on the order of $\Gamma^{(m)} \approx \hbar/\tau \sim 0.01-0.1$ eV and $V^{(ms)} \sim [\Gamma^{(m)}]^{1/2} \sim 0.1-0.3$ eV. Below, we use $V^{(ms)} = 0.004$ au ~ 0.11 eV.

(d) For the intermolecular interaction $V^{(m)}$, we use the estimate from ref 22 (based on ab initio calculations for 1,4-butanedithiol on gold(111)), $V^{(m)} = 0.0035$ au ~ 0.095 eV.

(e) Similarly, for the metal and the molecule−metal interaction, we use the same parameters that were used in ref 22. The tight binding metal interaction is taken as $V^{(t)} = 0.03$ au ~ 0.82 eV, and the molecule−metal interaction parameter is chosen to be $V^{(mt)} = 0.004$ au ~ 0.11 eV.

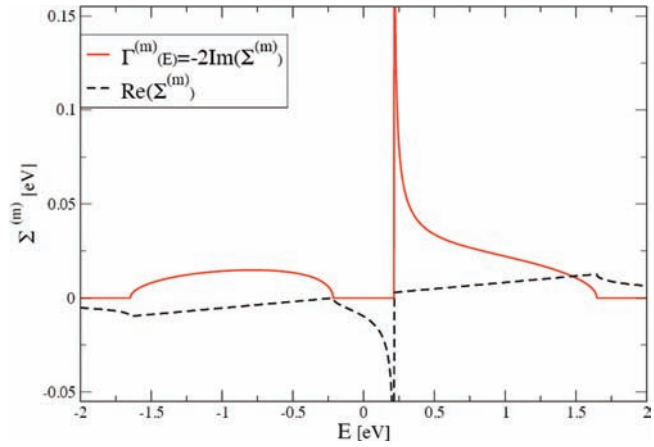

Figure 3. Real and imaginary parts of the self-energy of a molecular site adsorbed on a one-dimensional SC lattice, using the "standard" parameter set with the positive energy site at the SC surface. Full line (red): $\Gamma^{(m)}(E) = -2\mathrm{Im}(\Sigma^{(m)}(E))$; dashed line (black): $\mathrm{Re}(\Sigma^{(m)}(E))$.

(f) For the equilibrium junction, the metal site energy ε_t is set to 0, as is the SC mid-band gap. The molecular site energy is taken as $\varepsilon_m = -0.5$ eV. The choice of $\varepsilon_m = \varepsilon_t - 0.5$ eV corresponds to the observed order of magnitude of this difference in good molecular hole conductors.

In summary, the following set of "standard" interaction and energetic parameters are used in the calculation displayed and discussed below: $V^{(s)} = 0.82$ eV (the SC tight binding interaction), $V^{(t)} = 0.82$ eV (the metal TB interaction), $V^{(m)} = 0.095$ eV (intermolecular nearest-neighbor interaction within the molecular layer), molecule−metal and molecule−SC interactions, $V^{(mt)} = V^{(ms)} = 0.11$ eV, SC and metal site energies, $\varepsilon_s = \pm 0.215$ eV and $\varepsilon_t = 0$, respectively, and molecular site energy $\varepsilon_m = -0.5$ eV. It should be emphasized that this particular choice represents one reasonable scenario and that different junctions encompass a range of possible interaction parameters.

6. Results and Discussion

One-Dimensional Results. To gain insight into the site-alteration SC model, we start with the one-dimensional case. Figure 3 shows the imaginary (the spectral density (eq 11)) and real parts of the self-energy (eq 19a) associated with the adsorbate species using the "standard parameters" defined above and taking the "surface" SC site (on which the adsorbate is situated) to be of positive energy. These results are obtained using either the numerical or the analytical procedures described in section 2. As mentioned above, assigning the positive energy site to the SC surface removes symmetry about the energy origin, in contrast to ref 23 (a negative energy site at the SC surface will yield a mirror image of this picture). The corresponding result for the SC surface DOS, eq 23, is compared to the bulk DOS, eq 24, for the same model in Figure 4a. Here and below, the SC bands extend from $-2V^{(s)}d$ to $-\varepsilon_s$ and from ε_s to $2V^{(s)}d$, where d is the dimensionality. These results may be contrasted with their metallic counterparts (Figure 4b), obtained using the same model parameters except that $\varepsilon_s = 0$.

Three-Dimensional Results. The surface and bulk DOS, eq 38, of our "standard" 3-d SC model, averaged over positive and negative SC sites, are displayed in Figure 5. The two bands

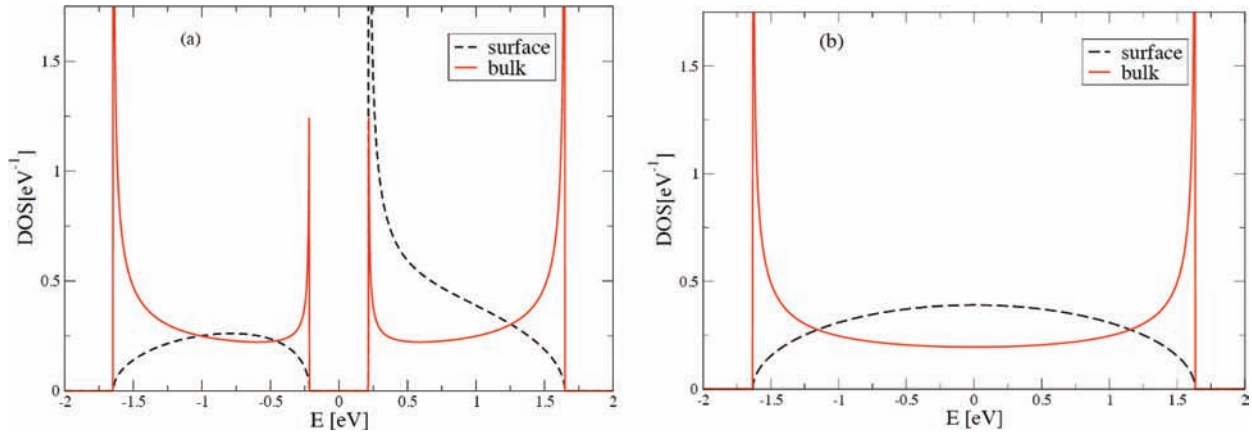

Figure 4. (a) Surface (full line, black) and bulk (dashed line, red) density of states, eqs 23 and 24, of the 1-d SC model with "standard" parameters and with the positive energy site at the SC surface. (b) The corresponding DOS functions for the metal obtained by setting $\varepsilon_s = 0$.

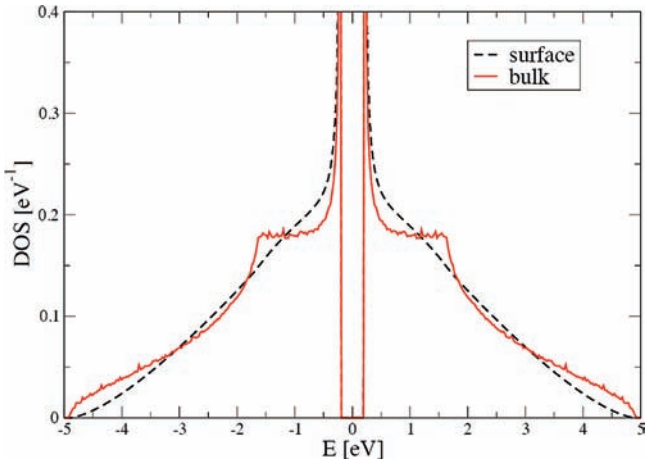

Figure 5. DOS of a three-dimensional SC surface (dashed line, black) and the bulk (full line, red). "Standard" parameters are used.

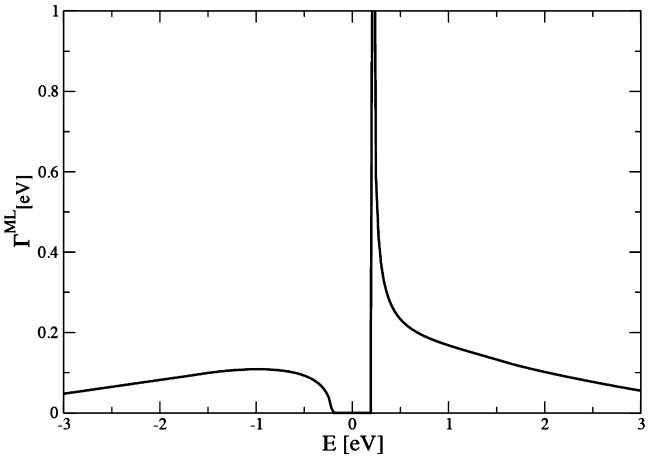

Figure 6. Local spectral density associated with an adsorbate species on top of a positive energy surface site of the SC surface. "Standard" parameters are used. A mirror image of this picture is obtained for an adsorbate situated on the negative energy site.

range from $-2V^{(s)}d$ to $-\varepsilon_s$ and from ε_s to $2V^{(s)}d$ (=4.92 eV). Figures 6−8 show spectral properties pertaining to molecules and molecular layers adsorbed on the surface of this model SC. The spectral function $\Gamma^{ML}_{\theta_{xy}}(E)$, eqs 34 and 37, calculated for one molecule from the molecular adsorbate layer chosen to sit on a positive energy surface site of our model

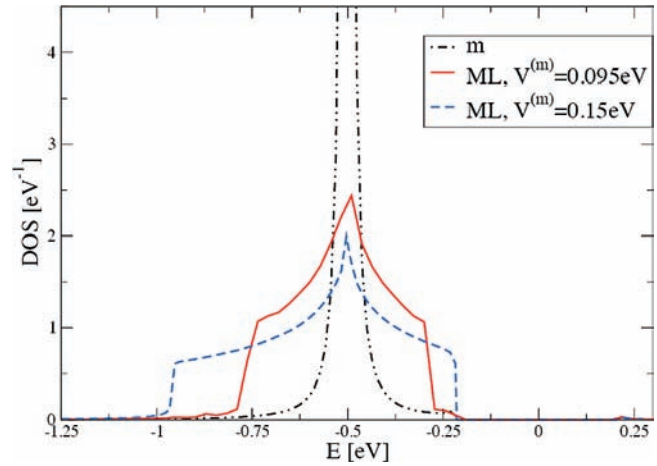

Figure 7. The density of states of a single molecule (m, dashed−dotted line, black) and a molecular layer (ML, full line, red, per molecule) adsorbed on the 3-d model SC, using the "standard" parameter set. Also shown (dashed line, blue) is the DOS for a molecular layer with "standard" parameters, except that the intermolecular interaction is taken to be 0.15 eV.

"standard" SC, is shown in Figure 6 (a mirror image of this picture is obtained for a molecule attached to a negative energy surface site).

In analyzing the density of states associated with adsorbate molecules, we distinguish between the local DOS associated with a molecule attached to a positive or negative energy site and the overall DOS characterizing the adsorbate layer, which, when displayed per adsorbate molecule, amounts to an average of DOS functions associated with surface sites of different (here, positive and negative) energies. The full line in Figure 7 shows the latter DOS function (per adsorbed molecule), eq 38c, for our "standard" system. In particular, in this case, the adsorbate intermolecular coupling is $V^{(m)} = 0.095$ eV. The dashed line represents a similar result for a larger coupling, $V^{(m)} = 0.15$ eV. These are compared to the corresponding result obtained for a single molecule (still averaged over positions above positive and negative energy SC surface sites), eq 40, using the "standard" parameters. The resulting DOS distributions are centered about the molecular site energy, $\varepsilon_m = -0.5$ eV, and their width is considerably larger for the layer and increases for a larger intermolecular interaction in this layer. Figure 8 shows DOS functions associated with a single molecule attached to the positive

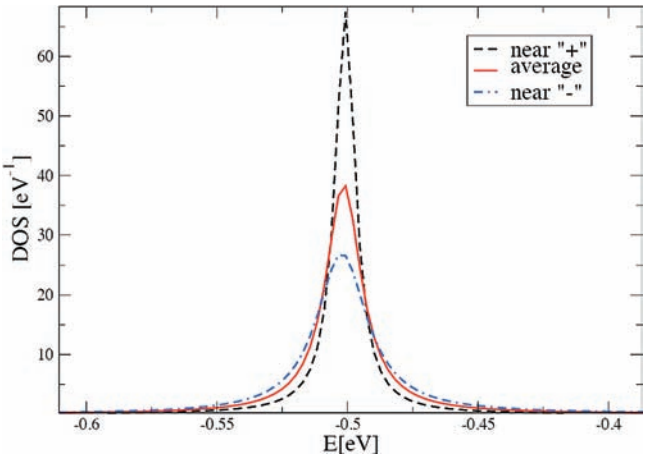

Figure 8. Full line (red): DOS of a single molecule adsorbed on a 3-d SC ("standard" parameters). The dashed−dotted (blue) and dashed (black) lines correspond to a molecule attached to a negative or positive energy SC surface site, respectively. The full line is the average of these two results.

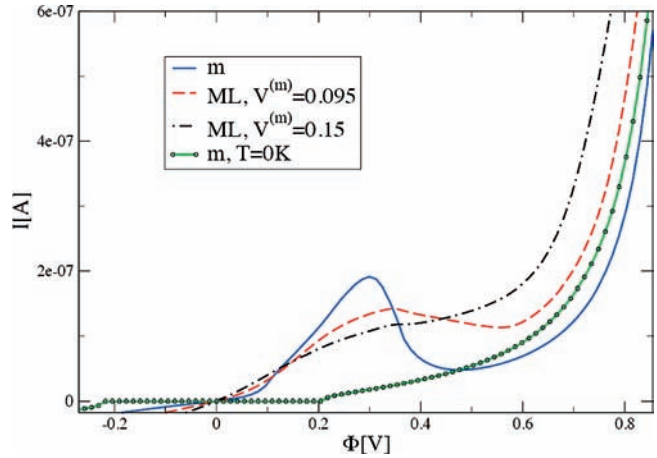

Figure 9. *I/V* curves for a metal−molecule−SC junction, using standard parameters at $T = 1200$ K and $S = 0.8$. Full line (blue): single molecule. Dashed line (red): a molecular layer ($V^{(m)} = 0.095$ eV). Dashed−dotted line (black): a molecular layer with the "standard" intermolecular interaction replaced by $V^{(m)} = 0.15$ eV. Also shown (full line with circles, green) is the $T = 0$ result (where NDR is absent) for the single-molecule junction.

and negative energy SC surface sites, as well as their average. Note that because the molecular site energy was taken to be −0.5 eV, the molecular DOS peak is considerably broader (and therefore lower at its maximum) for a molecule attached to a negative energy site, that is, interacting with a higher density of SC surface states.

Next, consider electron transmission and conductance. In ref 22, we have shown that broadening of the molecular spectrum due to intermolecular coupling in the adsorbate layer can strongly affect the current−voltage behavior of junctions involving such interfaces. In what follows, we focus on one particular characteristic of junctions involving semiconductors leads, reported and discussed in refs 7 and 8. When in the unbiased junction the bridge molecular level in a metal−molecule−SC junction lies just below the SC valence band edge (as well as below the metal Fermi energy), conductance may be nonzero at a finite temperature because of thermal depletion of electronic population from (i.e., hole generation in) the SC valence band. As the bias increases, the molecular level may shift past the valence band edge and enter into the SC band gap, leading to current reduction, which amounts to negative differential resistance (NDR). When the voltage increases further, the molecular level further enters the SC conduction band, and current increase resumes.

The possibility of observing this kind of behavior, or more generally the manifestation of the spectral density associated with the molecule−SC interaction in the junction transport behavior, depends sensitively on the way in which the adsorbate level(s) shifts with bias relative to the SC electronic structure. Indeed, Quek et al.[33] argue against the mechanism proposed in refs 7 and 8 applied to the cyclopentene on p-type Si(001) system, based on ab initio calculations of the voltage-induced energy shifts involved. In the following, we consider a metal−molecule (molecular layer)−semiconductor junction with the "standard" parameter set and use eq 46 with S chosen as detailed in the figure captions. Figures 9 and 10 show the effect of intermolecular interactions in the adsorbate layer on this NDR behavior. Figure 9 compares the behavior of a single-molecule junction and of a junction comprising a molecular layer with different intermolecular interactions, as in Figure 7. A strong NDR effect at $T = 1200$ K, seen in the single-molecule junction, becomes much milder in the molecular layer case and all but disappears when the intermolecular interaction $V^{(m)}$ becomes larger and the spectral width characterizing the molecular layer exceeds the SC band gap. ($T = 1200$ K may appear to be a high

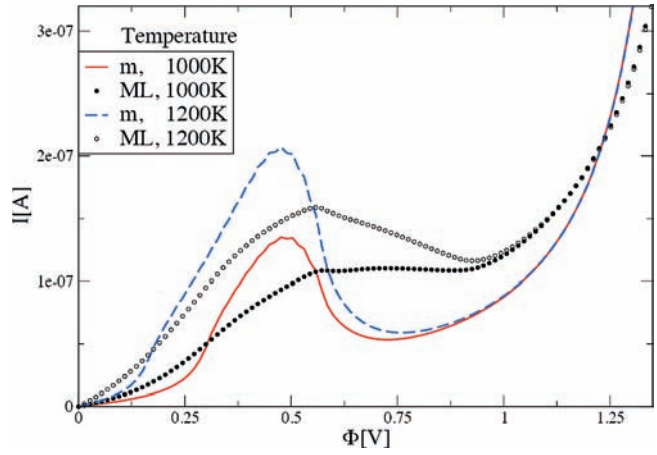

Figure 10. *I/V* curves for a metal−molecule−SC junctions, using standard parameters and $S = 0.5$, calculated at $T = 1000$ K (molecular layer and single molecule results displayed using full circles (black) and a full line (red), respectively) and at $T = 1200$ K (a dashed (blue) line for the single-molecule junction; empty circles (black) for the molecular layer).

temperature, but our model is only expected to yield qualitative understanding. Also, the temperature used merely reflects the number of holes in the SC valence band, arising from the Fermi functions in eq 45. The same hole concentration may be obtained at a much lower temperature using doping.) The same behavior is seen from another point of view in Figure 10, which compares the behavior of a single-molecule junction and that of a junction based on a molecular layer at two different temperatures. The NDR behavior is considerably less pronounced at the lower temperature and disappears altogether for the molecular layer case.

7. Conclusions

In this paper, we applied a generic minimal tight binding model to compare electronic spectral and transport properties of molecules and molecular layers adsorbed on semiconductor surfaces and used as bridges in semiconductor-based molecular junctions. The semiconductor model is based on a site-alteration model where a two-band electronic structure results from a

periodic array of unit cells with two sites characterized by different energies. Our analytical results in one dimension provide a generalization of the Newns semielliptic spectral function[24] that characterizes a simple tight binding model metal and yield this result in the appropriate limit. Numerical evaluation based on a renormalization group algorithm is verified by comparing to these 1-d results and is then used in the corresponding three-dimensional model. The resulting spectral functions and density of states are dominated by a prominent band gap that strongly affects the transport properties of junctions based on such SC lead(s).

As in our previous study, where we compared single-molecule junctions to junctions based on molecular layers or molecular islands between two metal electrodes, we find that within our simple model, the main effect of increasing the number of interacting molecules stems from broadening of the effective molecular DOS and consequently the conduction spectrum. In particular, we focused on the finite-temperature NDR phenomenon associated with the voltage-induced shift of the conducting molecule across the SC valence band edge into the gap. We found that intermolecular interactions can strongly reduce and even eliminate the NDR feature.

It should be kept in mind that intermolecular interactions treated at the tight binding level are only one source of adsorbate cooperative behavior in molecular conduction. On semiconductor substrates, important electrostatic effects associated with permanent molecular dipoles[34] as well as with charge transfer between molecules and the substrate[35] may dominate the junction behavior. A complete picture of molecular coverage effects in molecular transport junctions should account for such effects as well.

Acknowledgment. A.N.'s research is supported by the Israel Science Foundation, the German−Israel Foundation, and the European Research Comission. L.K.'s research is supported by the Israel Science Foundation and the Lise Meitner Center for Computational Chemistry. This paper is dedicated to Prof. Benny Gerber, a friend, colleague, and a leader in our field.

Appendix A

Equation 6 can be recast as

$$x = \pm\sqrt{\varepsilon_s^2 + 4(V^{(s)})^2\cos^2(\theta)} \tag{A1}$$

where $x \equiv E_{\theta\pm}$. This yields

$$d\theta = -dx\frac{x}{4(V^{(s)})^2\cos(\theta)\sin(\theta)} \tag{A2}$$

Using eq A2 in eq 9 gives

$$\Gamma^{(m)}(x) = -8|V^{(ms)}|^2\int dx\frac{x\cos(\theta)\sin(\theta)}{(x-\varepsilon_s)^2 + 4(V^{(s)})^2\cos^2(\theta)}\delta(E-x) \tag{A3}$$

Inserting eq A1 into eq A3 yields, after some straightforward algebraic manipulation

$$\begin{aligned}\Gamma^{(m)}(x) &= -8|V^{(ms)}|^2\int dx\frac{x\sqrt{\frac{x^2-\varepsilon_s^2}{4(V^{(s)})^2}}\sqrt{1-\frac{x^2-\varepsilon_s^2}{4(V^{(s)})^2}}}{(x-\varepsilon_s)^2 + 4(V^{(s)})^2\frac{x^2-\varepsilon_s^2}{4(V^{(s)})^2}}\delta(E-x)\\ &= -4|V^{(s)}|^2\int dx\frac{\sqrt{\frac{x^2-\varepsilon_s^2}{4(V^{(s)})^2} - \left(\frac{x^2-\varepsilon_s^2}{4(V^{(s)})^2}\right)^2}}{x-\varepsilon_s}\delta(E-x)\end{aligned} \tag{A4}$$

Because $0 \le \theta < \pi/2$, eq A1 implies that x must assume real positive values for $\varepsilon_s \le x < [\varepsilon_s^2 + 4(V^{(s)})^2]^{1/2}$ and real negative values for $-[\varepsilon_s^2 + 4(V^{(s)})^2]^{1/2} \le x < -\varepsilon_s$. Using these limits in the integral of eq A4 yields

$$\begin{aligned}\Gamma^{(m)}(x) = -4|V^{(ms)}|^2 &\left[\int_{\sqrt{\varepsilon_s^2+4(V^{(s)})^2}}^{\varepsilon_s} dx\frac{\sqrt{\frac{x^2-\varepsilon_s^2}{4(V^{(s)})^2} - \left(\frac{x^2-\varepsilon_s^2}{4(V^{(s)})^2}\right)^2}}{x-\varepsilon_s}\delta(E-x) + \right.\\ &\left.\int_{-\sqrt{\varepsilon_s^2+4(V^{(s)})^2}}^{-\varepsilon_s} dx\frac{\sqrt{\frac{x^2-\varepsilon_s^2}{4(V^{(s)})^2} - \left(\frac{x^2-\varepsilon_s^2}{4(V^{(s)})^2}\right)^2}}{x-\varepsilon_s}\delta(E-x)\right]\end{aligned} \tag{A5}$$

Appendix B

Here, we provide explicit expressions for the block Hamiltonian terms in eq 31. In terms of the energetic parameters that define our tight binding model for a molecular monolayer adsorbed on the surface of a cubic SC, they are given by

$$\mathbf{H}_{00}^{SC}(\boldsymbol{\theta}_{xy}) = \begin{pmatrix} \varepsilon_s & V^{(s)}(1+e^{-i2\theta_x}) & V^{(s)}(1+e^{i2\theta_y}) & 0 & V^{(s)} & 0 & 0 & 0 \\ V^{(s)}(1+e^{i2\theta_x}) & -\varepsilon_s & 0 & V^{(s)}(1+e^{i2\theta_y}) & 0 & V^{(s)} & 0 & 0 \\ V^{(s)}(1+e^{-i2\theta_y}) & 0 & -\varepsilon_s & V^{(s)}(1+e^{-i2\theta_x}) & 0 & 0 & V^{(s)} & 0 \\ 0 & V^{(s)}(1+e^{-i2\theta_y}) & V^{(s)}(1+e^{i2\theta_x}) & \varepsilon_s & 0 & 0 & 0 & V^{(s)} \\ V^{(s)} & 0 & 0 & 0 & -\varepsilon_s & V^{(s)}(1+e^{-i2\theta_x}) & V^{(s)}(1+e^{i2\theta_y}) & 0 \\ 0 & V^{(s)} & 0 & 0 & V^{(s)}(1+e^{i2\theta_x}) & \varepsilon_s & 0 & V^{(s)}(1+e^{i2\theta_y}) \\ 0 & 0 & V^{(s)} & 0 & V^{(s)}(1+e^{-i2\theta_y}) & 0 & \varepsilon_s & V^{(s)}(1+e^{-i2\theta_x}) \\ 0 & 0 & 0 & V^{(s)} & 0 & V^{(s)}(1+e^{-i2\theta_y}) & V^{(s)}(1+e^{i2\theta_x}) & -\varepsilon_s \end{pmatrix} \tag{B1}$$

$$\mathbf{H}_{01}^{\mathrm{SC}} = \begin{pmatrix} 0 & 0 & 0 & 0 & 0 & 0 & 0 & 0 \\ 0 & 0 & 0 & 0 & 0 & 0 & 0 & 0 \\ 0 & 0 & 0 & 0 & 0 & 0 & 0 & 0 \\ 0 & 0 & 0 & 0 & 0 & 0 & 0 & 0 \\ V^{(\mathrm{s})} & 0 & 0 & 0 & 0 & 0 & 0 & 0 \\ 0 & V^{(\mathrm{s})} & 0 & 0 & 0 & 0 & 0 & 0 \\ 0 & 0 & V^{(\mathrm{s})} & 0 & 0 & 0 & 0 & 0 \\ 0 & 0 & 0 & V^{(\mathrm{s})} & 0 & 0 & 0 & 0 \end{pmatrix} \tag{B2}$$

$$\mathbf{H}^{\mathrm{ML}}(\boldsymbol{\theta}_{xy}) = \begin{pmatrix} \varepsilon_{\mathrm{m}} & V^{(\mathrm{m})}(1 + \mathrm{e}^{-\mathrm{i}2\theta_x}) & V^{(\mathrm{m})}(1 + \mathrm{e}^{\mathrm{i}2\theta_y}) & 0 \\ V^{(\mathrm{m})}(1 + \mathrm{e}^{\mathrm{i}2\theta_x}) & \varepsilon_{\mathrm{m}} & 0 & V^{(m)}(1 + \mathrm{e}^{\mathrm{i}2\theta_y}) \\ V^{(\mathrm{m})}(1 + \mathrm{e}^{-\mathrm{i}2\theta_y}) & 0 & \varepsilon_{\mathrm{m}} & V^{(\mathrm{m})}(1 + \mathrm{e}^{-\mathrm{i}2\theta_x}) \\ 0 & V^{(\mathrm{m})}(1 + \mathrm{e}^{-\mathrm{i}2\theta_y}) & V^{(\mathrm{m})}(1 + \mathrm{e}^{\mathrm{i}2\theta_x}) & \varepsilon_{\mathrm{m}} \end{pmatrix} \tag{B3}$$

and

$$\mathbf{H}^{\mathrm{MS}} = \begin{pmatrix} V^{(\mathrm{ms}+)} & 0 & 0 & 0 & 0 & 0 & 0 & 0 \\ 0 & V^{(\mathrm{ms}-)} & 0 & 0 & 0 & 0 & 0 & 0 \\ 0 & 0 & V^{(\mathrm{ms}-)} & 0 & 0 & 0 & 0 & 0 \\ 0 & 0 & 0 & V^{(\mathrm{ms}+)} & 0 & 0 & 0 & 0 \end{pmatrix} \tag{B4}$$

References and Notes

(1) Wolkow, R. A. *Jpn. J. Appl. Phys.* **2001**, *40*, 4378.

(2) Guisinger, N. P.; Basu, R.; Baluch, A. S.; Hersam, M. C. *Ann. N.Y. Acad. Sci.* **2003**, *1006*, 227.

(3) Guisinger, N. P.; Greene, M. E.; Basu, R.; Baluch, A. S.; Hersam, M. C. *Nano Lett.* **2004**, *4*, 55.

(4) Guisinger, N. P.; Basu, R.; Greene, M. E.; Baluch, A. S.; Hersam, M. C. *Nanotechnology* **2004**, *15*, S452.

(5) Lenfant, S.; Krzeminski, C.; Delerue, C.; Allan, G.; Vuillaume, D. *Nano Lett.* **2003**, *3*, 741.

(6) McCreery, L. *Chem. Mater.* **2004**, *16*, 4477.

(7) Rakshit, T.; Liang, G.-C.; Ghosh, A. W.; Datta, S. *Nano Lett.* **2004**, *4*, 1803.

(8) Rakshit, T.; Liang, G. C.; Ghosh, A. W.; Hersam, M. C.; Datta, S. *Phys. Rev. B* **2005**, *72*, 125305.

(9) Lodha, S.; Janes, D. B. *J. Appl. Phys.* **2006**, *100*, 024503.

(10) Adam, J. D.; Robert, A. W. *Phys. Rev. B* **2008**, *77*, 115305.

(11) Nesher, G.; Vilan, A.; Cohen, H.; Cahen, D.; Amy, F.; Chan, C.; Hwang, J. H.; Kahn, A. *J. Phys. Chem. B* **2006**, *110*, 14363.

(12) Nesher, G.; Shpaisman, H.; Cahen, D. *J. Am. Chem. Soc.* **2007**, *129*, 734.

(13) Salomon, A.; Boecking, T.; Seitz, O.; Markus, T.; Amy, F.; Chan, C.; Zhao, W.; Cahen, D.; Kahn, A. *Adv. Mater.* **2007**, *19*, 445–450.

(14) Thieblemont, F.; Seitz, O.; Vilan, A.; Cohen, H.; Salomon, E.; Kahn, A.; Cahen, D. *Adv. Mater.* **2008**, *20*, 3931–3936.

(15) Hsu, J. W. P.; Lang, D. V.; West, K. W.; Loo, Y. L.; Halls, M. D.; Raghavachari, K. *J. Phys. Chem. B* **2005**, *109*, 5719.

(16) Yu, L. H.; Gergel-Hackett, N.; Zangmeister, C. D.; Hacker, C. A.; Richter, C. A.; Kushmerick, J. G. *J. Phys.: Condens. Matter* **2008**, *20*, 374114.

(17) Scott, A.; Janes, D. B.; Risko, C.; Ratner, M. A. *Appl. Phys. Lett.* **2007**, *91*, 033508.

(18) Wang, W.; Scott, A.; Gergel-Hackett, N.; Hacker, C. A.; Janes, D. B.; Richter, C. A. *Nano Lett.* **2008**, *8*, 478.

(19) Seitz, O.; Böcking, T.; Salomon, A.; Gooding, J. J.; Cahen, D. *Langmuir* **2006**, *22*, 6915.

(20) Maldonado, S.; Knapp, D.; Lewis, N. S. *J. Am. Chem. Soc.* **2008**, *130*, 3300.

(21) Kümmel, S.; Kronik, L. *Rev. Mod. Phys.* **2008**, *80*, 3.

(22) Landau, A.; Kronik, L.; Nitzan, A. *J. Comput. Theor. Nanosci.* **2008**, *5*, 535.

(23) Mujica, V.; Ratner, M. A. *Chem. Phys.* **2006**, *326*, 197.

(24) Newns, D. M. *Phys. Rev.* **1969**, *178*, 1123.

(25) Guinea, F.; Tejedor, T.; Flores, F.; Louis, E. *Phys. Rev. B* **1983**, *28*, 4397.

(26) Lopez-Sancho, M. P.; Lopez-Sancho, L. M.; Rubio, J. *J. Phys. F: Met. Phys.* **1984**, *14*, 1205.

(27) Lopez-Sancho, M. P.; Lopez-Sancho, L. M.; Rubio, J. *J. Phys. F: Met. Phys.* **1985**, *15*, 851.

(28) Galperin, M.; Toledo, S.; Nitzan, A. *J. Chem. Phys.* **2002**, *117*, 10817.

(29) Galperin, M.; Nitzan, A.; Benjamin, I. *J. Phys. Chem. A* **2002**, *106*, 10790.

(30) Eastman, D. E.; Grobman, W. D.; Freeouf, J. L.; Erbudak, M. *Phys. Rev. B* **1974**, *9*, 3473.

(31) Chelikowsky, J. R.; Cohen, M. L. *Phys. Rev. B* **1976**, *14*, 556.

(32) Schnadt, J.; Bruhwiler, P. A.; Patthey, L.; O'Shea, J. N.; Sodergren, S.; Odelius, M.; Ahuja, R.; Karis, O.; Bassler, M.; Persson, P.; Siegbahn, H.; Lunell, S.; Martensson, N. *Nature* **2002**, *418*, 620.

(33) Quek, S. Y.; Neaton, J. B.; Hybertsen, M. S.; Kaxiras, E.; Louie, S. G. *Phys. Rev. Lett.* **2007**, *98*, 066807.

(34) Natan, A.; Kronik, L.; Haick, H.; Tung, R. T. *Adv. Mater.* **2007**, *19*, 4103.

(35) Cahen, D.; Naaman, R.; Vager, Z. *Adv. Funct. Mater.* **2005**, *15*, 1571.

JP900301F